

Miniaturized-Element Frequency Selective Surfaces for Millimeter-Wave to Terahertz Applications

Meysam Moallem, *Student Member, IEEE*, and Kamal Sarabandi, *Fellow, IEEE*

Abstract—This paper presents a single-face, membrane-supported, miniaturized-element frequency selective surface (MEFSS) for image rejection of a J -band upconverter mixer. In this design, a new miniaturized-element patch-wire MEFSS configuration is proposed to select the upper-side band (USB) response of a wave radiated from an upconverter. The proposed MEFSS produces a single pole and an adjacent transmission zero to suppress the lower sideband. It is shown that the frequency response of this MEFSS can be predicted by an equivalent circuit model and that the location of pole and zero can be tuned independently with physical parameters. MEFSS elements are supported and protected by a 10 μm thick low-loss polymer membrane which allows flexible handling and minimizes substrate losses. Thickness of the metallic traces is increased to reduce the conductor loss. A salient feature of this design is low sensitivity of its frequency response to the angle of incidence and the absence of a harmonic response. This feature allows placement of the spatial filter in close proximity to radiating elements with spherical wavefronts. The membrane-supported MEFSS is fabricated using a microfabrication method with tolerances that allow such filter implementations up to terahertz frequencies. Performance of the fabricated device is experimentally verified using a free-space measurement setup. Experimental results show that the transmission response has 0.6 dB insertion loss in the passband (221–223 GHz) and more than 25 dB rejection out-of-band (206–208 GHz) which is in good agreement with full-wave simulation and its circuit model prediction.

Index Terms—Miniaturized-element frequency selective surface (MEFSS), single-side band filter, millimeter-wave (MMW), microfabrication technology.

I. INTRODUCTION

IN RECENT years, millimeter-wave (MMW) radars have been widely investigated for collision avoidance and imaging applications [1]–[3]. Reduction in size and mass of the radar while maintaining a certain angular resolution and the ability to see through optically opaque atmospheric conditions are among the important advantages of radars operating at higher millimeter-wave through terahertz frequency bands. These radars typically have a harmonic mixer at the last stage to upconvert a modulated IF signal to the desired RF transmit frequency. Harmonic mixer nonlinear intermodulation creates

Manuscript received December 07, 2011; revised February 10, 2012; accepted February 16, 2012. Date of publication May 01, 2012; current version May 08, 2012. This work was supported by the U.S. Army Research Laboratory under Contract W911NF and prepared through collaborative participation in the Microelectronics Center of Micro Autonomous Systems and Technology (MAST) Collaborative Technology Alliance (CTA).

The authors are with the Department of Electrical Engineering and Computer Science, The University of Michigan at Ann Arbor, Ann Arbor, MI 48109 USA (e-mail: moallem@umich.edu).

Color versions of one or more of the figures in this paper are available online at <http://ieeexplore.ieee.org>.

Digital Object Identifier 10.1109/TTHZ.2012.2189910

different mixing products of LO and IF signals. Among these signals, the image signal has the highest amplitude and is downconverted into the same band as the RF signal. Mixture of these signals in the receiver can cause a significant error in radar measurements. To avoid measurement errors, a bandpass filter is required to provide high isolation between adjacent bands of the RF signal and its image. Waveguide and planar MMIC filters have been traditionally used in communication and radar systems [4], [5] to achieve band isolation between different channels. To achieve channel selection between adjacent bands, high order filters are required to achieve the necessary suppression of the undesired sideband. The design and realization of multipole filters at high millimeter- and submillimeter-wave frequencies is very difficult and leads to higher than desired insertion loss. Planar MMIC filters, on the other hand, are easy to fabricate but their loss is prohibitively high for most radar and communication applications at these high frequencies.

Frequency selective surface (FSS) structures have been utilized in millimeter- and submillimeter-wave remote sensing instruments to provide spatial filtering [6]–[8]. Multilayer resonant-element FSSs are reported with low insertion losses (as low as 0.6 dB) and 30 dB isolation in adjacent bands with a band separation of 1:1.07 [6], [7]. One common feature among traditional resonant FSS structures is that the size of the resonant elements and their spacing are comparable to the wavelength at the operating frequency. The frequency response of these structures is the result of mutual interactions of many adjacent unit cells and energy coupling of many slowly decaying evanescent Bragg modes. Hence, in order to observe the desired frequency response, the surface must include a large number of resonant elements and be illuminated by a planar phase front at a particular designed angle of incidence. Hence for certain applications FSS structures with relatively small electrical dimensions that are less sensitive to the incidence angle and can operate with non-planar phase fronts are highly desirable. A new class of FSSs called miniaturized-element FSSs (MEFSS) was introduced in [9]. The MEFSSs consist of a multilayer periodic array of metallic structures with dimensions that are much smaller than the wavelength at the operating frequency. This design allows for localization of bandpass characteristics to a small area on the surface, which allows flexible spatial filtering for an arbitrary wave phase front. Another advantage of the miniaturized-element design lies in the fact that the interaction of the surface and incident plane wave is predominantly in the TEM mode. As a result, higher order Bragg modes are suppressed, and harmonic responses are eliminated. In addition, the interaction of these MEFSS structures with an incident electromagnetic wave can be modeled as lumped inductive and capacitive elements. This allows for design and tuning of MEFSS structures with arbitrary frequency

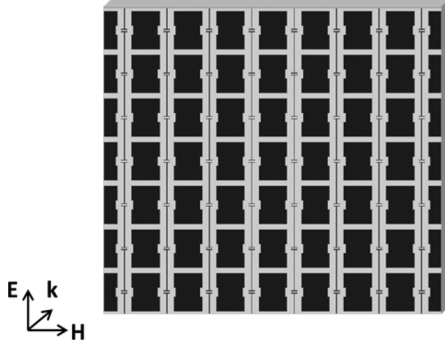


Fig. 1. Proposed single face, membrane supported, MEFSS illuminated by a vertically polarized plane wave.

responses based on their equivalent circuit model. In recent years, numerous variations of the miniaturized-element FSSs have been reported with operating frequencies up to 26 GHz [10], [11]. Single and multilayer multipole MEFSSs are fabricated using standard printed circuit board (PCB) technology at these frequency bands.

The work presented in this paper is motivated by the need for a high isolation between upper-side band (UPS) and lower-side band (LSB) signals present in the output spectrum of a *Y*-band instrumentation radar [12]. The filter objective is to provide minimum insertion loss in the 221–223 GHz band and more than 25 dB signal suppression in the 205–207 GHz band. In addition, the spatial filter needs to be placed at a small distance from the radar feed antenna where we have a spherical phase front. A new MEFSS consisting of arrays of patch and I-shaped wires, as shown in Fig. 1, is proposed to meet the required filtering characteristics for a vertically polarized incident wave. In this design, metallic elements are supported on a thin membrane sheet. In Section II, the design procedure based on the equivalent circuit model is described and a full-wave numerical analysis is performed to verify the model accuracy. Sources of loss have been analyzed to improve the insertion loss and the out of band rejection of the MEFSS. It will be shown that the transmission response of the proposed FSS has small dependency on the angle of incidence near the normal direction. Section III describes the MEFSS fabrication process using a microfabrication technique. In Section IV, the experimental response of the fabricated prototype is presented using a free-space millimeter-wave measurement setup. Finally, a summary of the work is presented in Section V.

II. DESIGN AND EQUIVALENT CIRCUIT MODEL DEVELOPMENT OF PATCH-WIRE MEFSS

To achieve the desired filtering response using a simple structure with a low insertion loss, a single pole filter with an adjacent transmission zero is considered. This simple filtering response can be obtained from the circuit model shown in Fig. 2. Such a circuit can easily be realized in terms of a MEFSS structure. The configuration of such a MEFSS is shown in Fig. 3. Basically, the I-shaped elements interact with a V-polarized wave and behave as a series *L*-*C* branch. The inductance is a function of the length, width, and thickness (D_y, w_L, t_m) of the wire section, while the capacitance is mainly affected by the gap between two adjacent caps (s). The spacing between the I-shaped

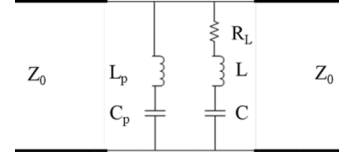


Fig. 2. Equivalent circuit model of the MEFSS for a vertically polarized wave front at a normal incident angle. $L = 0.5837$ nH, $C = 1.0105$ fF, $C_p = 7.147$ fF, $L_p = 0.0166$ nH, $R_L = 6.4479$ Ω , $Z_0 = 377$ Ω .

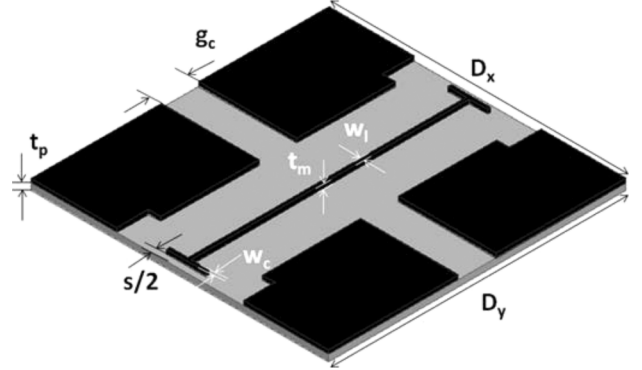


Fig. 3. A unit cell of the MEFSS. $D_x = D_y = 470$ μm , $g_c = 60$ μm , $s = 20$ μm , $t_m = 7$ μm , $w_1 = 5.7$ μm , $w_c = 5$ μm , $t_p = 10$ μm .

elements and patches can affect the inductance of the I-shaped elements if it becomes small enough. Basically the inductance of the I-shaped elements decreases as the metallic patch gets too close because it suppresses the circulating magnetic field around the wire. The patch array is modeled by a capacitor which is in parallel with the *L*-*C* branch. The patch capacitor value, C_p , is a function of the gap between adjacent elements (g_c) and the dielectric constant of the supporting membrane. The patch elements create a small inductance which is modeled as an inductor, L_p , in series with C_p . As mentioned before, the circuit model has a passband frequency and an adjacent transmission zero frequency in its transmission response. There is also a second zero associated with the L_p - C_p branch which occurs at a much higher frequency compared to the other two resonant frequencies. Since $\omega L \gg R_L$ (R_L represents the wire resistance), these resonant frequencies are approximately equal to:

$$\omega_{z1} = \frac{1}{\sqrt{LC}} < \omega_p = \frac{1}{\sqrt{(L + L_p) \frac{CC_p}{C + C_p}}} \ll \omega_{z2} = \frac{1}{\sqrt{L_p C_p}}. \quad (1)$$

It is noted that the pole frequency (ω_p) is always larger than the first transmission zero frequency (ω_{z1}) which is desired to suppress the LSB of the mixer. All the lumped element values in the model can be tuned independently using elements dimensions in the structure. This provides flexibility in adjusting the resonant frequencies in the transmission response by changing the dimensions of the structure. ω_{z1} is determined by the dimensions of the I-shaped elements. Considering $L_p \ll L$, ω_p can be defined as a function of ω_{z1} as follow:

$$\frac{\omega_p}{\omega_{z1}} = \sqrt{1 + \frac{C}{C_p}} \quad (2)$$

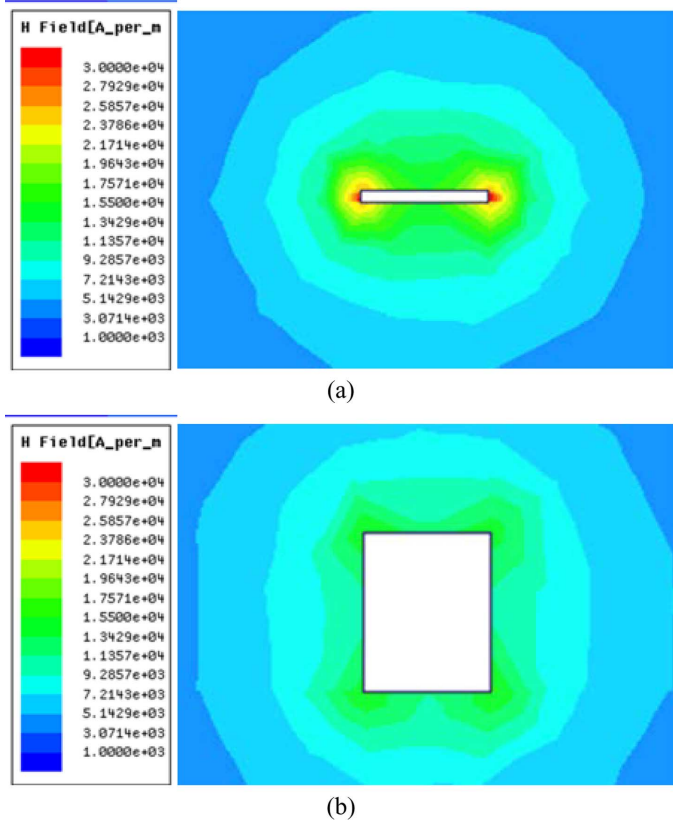


Fig. 4. Magnetic field distribution around a wire element for two different thicknesses: (a) $t_m = 0.5 \mu\text{m}$ (b) $t_m = 7 \mu\text{m}$.

Hence, the passband frequency can be pushed as close as desired to the first transmission zero by increasing C_p , or equivalently reducing g_c , without changing the transmission zero frequency.

In submillimeter-wave frequencies and higher, two main sources of loss, namely substrate loss and conductor loss, limit the performance of spatial filters by increasing the insertion loss and decreasing the rejection in the transmission response. The dielectric substrate increases insertion loss by creating an impedance mismatch with free space. In addition, the dielectric loss in the substrate can become large in these frequency bands. To reduce losses associated with the substrate, the MEFSS is designed on a $10 \mu\text{m}$ thick ($\sim \lambda/80$) Parylene membrane. Excellent physical and electrical properties such as low intrinsic thin film stress, homogeneous surface and low dielectric constant, makes Parylene suitable for this application. Large areas of a thin layer of Parylene can be released and handled which makes it ideal for freestanding structures. The low dielectric constant and loss tangent ($\epsilon_r = 2.9 @ 1 \text{ MHz}$, $\tan \delta = 0.004 @ 60 \text{ GHz}$ [13]) of Parylene is desirable to reduce the mismatch and dielectric loss of the FSS structure.

Ohmic loss in the metallic elements is another source of loss which increases the insertion loss in the passband and reduces the rejection in the bandstop. This loss is modeled as a resistance R_L in series with the inductor in the circuit model. This loss is a function of the surface resistivity of the metal strips and the current distribution on the wire elements. Gold has a high bulk conductivity ($\sigma = 4.1 \times 10^7 \text{ S/m}$) and its surface resistivity is $R_s = 0.146 \Omega$ at 220 GHz . However, similar to planar

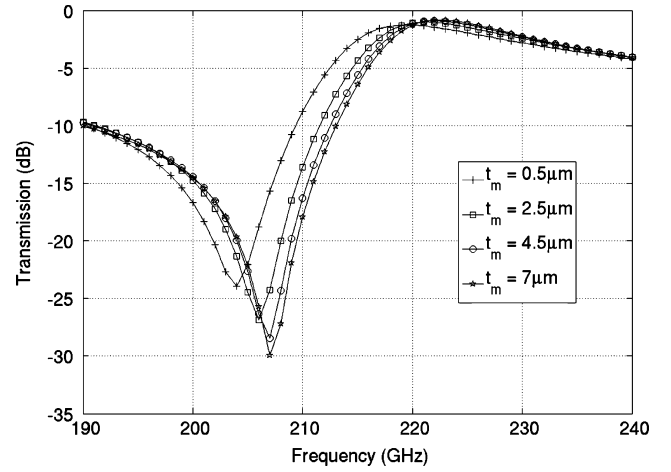


Fig. 5. Simulation results for the patch-wire MEFSS with different element thicknesses. The insertion loss in the passband and the rejection out of the band improves as the element thicknesses increase.

transmission lines, e.g., microstrips and coplanar waveguides, the induced currents are not uniformly distributed on the wire strip surface, as they are mostly concentrated near the edges of the strips. This effect is due to the singular behavior of the electromagnetic field near a conductor wedge [14]. Fig. 4 shows the magnetic field distribution around the wire element. The surface current density is equal to the tangential component of the magnetic field. To reduce the current density on the edges and increase the effective surface of the strip, the curvature of the strips near the edges must be reduced. This can be done essentially by increasing the thickness of the strips. Numerical simulations verify that the current distribution is much more uniform on a thick strip as shown in Fig. 4(b). Fig. 5 shows that the insertion loss and isolation are improved as a result of increasing the wire thickness.

Full-wave analysis of the structure was performed in a commercial finite-element method solver (Ansoft HFSS). A single unit cell (Fig. 3) is excited by Floquet ports and the reflection (S11) and transmission (S21) responses of the proposed MEFSS are computed. Master and slave boundaries are incorporated to model the planes of periodicity for the array and to ensure phase continuity across the unit cells for a desired angle of incidence. The transmission response of the FSS as a function of angle of incidence is shown in Fig. 6. As shown, the transmission response is not very sensitive to the angle of incidence. Resonant frequencies shift by 1% and 5% for angles of incidence equal to 20° and 50° , respectively, with respect to the normal direction.

The equivalent circuit model is simulated with Advanced Design System (ADS). The circuit parameters have been optimized to fit the full-wave analysis results. The lumped-element model is valid so long as the interaction of the FSS elements and the incident wave remains mostly in TEM mode. The first Bragg mode contribution starts to come to effect when the periodicity approaches $\lambda/2$. As the frequency increases and the unit cell dimensions become comparable to the wavelength, the lumped-element circuit model accuracy drops, especially for oblique angles of incidence. Fig. 7 shows the reflection and transmission responses of the optimized structure and the equivalent circuit model up to 450 GHz . The responses are in close agreement over the entire band. It can also be noted that the second harmonic

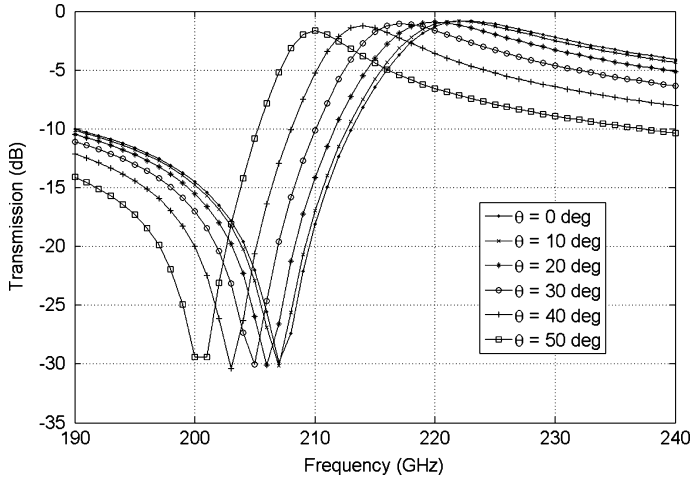


Fig. 6. Simulation results of the patch-wire MEFSS for different angles of incidence.

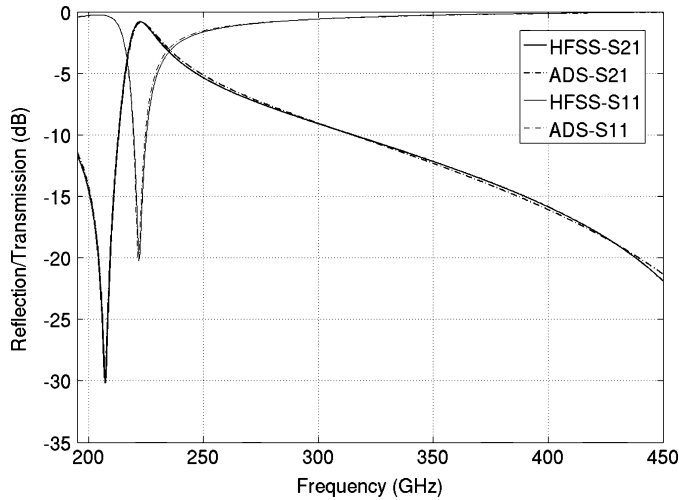


Fig. 7. Numerical simulations for patch-wire MEFSS at normal incidence. There is good agreement between the structure and the circuit model simulation results in the operating frequency band.

response is not present (at 414–444 GHz) unlike an equivalent resonant FSS structure design.

The structure dimensions can be scaled to create the same filtering response at higher submillimeter-wave and terahertz frequencies. Full-wave simulation results for the scaled MEFSS structures are shown in Fig. 8. It can be seen that the scaled structures create a filtering response with characteristics identical to the original structure in the corresponding bands. The insertion loss and LSB rejection are slightly worsened as the operating frequency increases due to higher conductor loss on the metallic traces.

III. FABRICATION PROCESS

The membrane-supported FSS structure was fabricated using wafer microfabrication technology. The fabrication process consists of three major steps: deposition of a thin Parylene sheet on a carrier wafer, pattern and growth of miniaturized elements over the Parylene layer, and release of the Parylene-supported structure from the carrier wafer. More detail steps in the fabrication process are shown in Fig. 9. First, a bare polished silicon

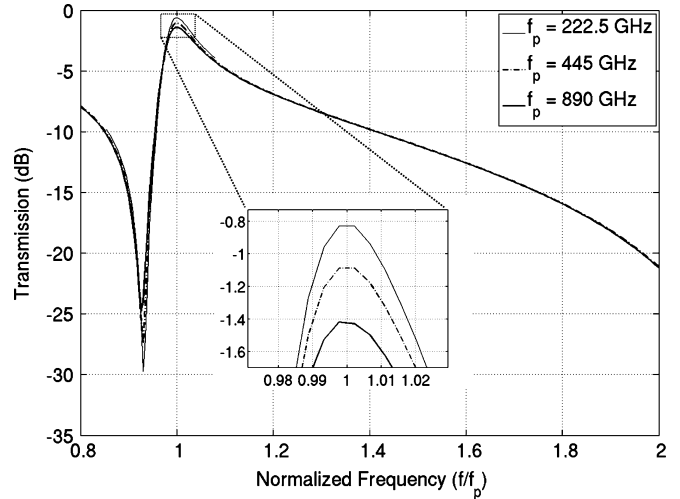


Fig. 8. Full-wave simulation of the scaled MEFSS for terahertz applications.

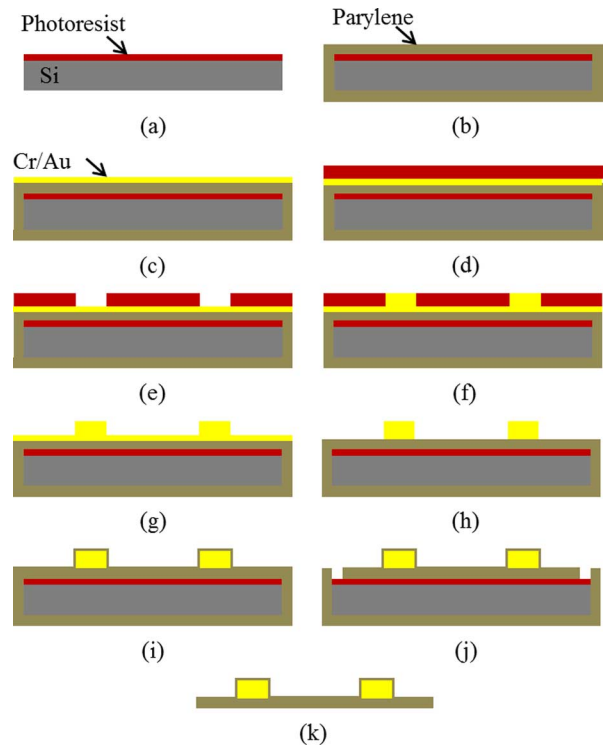


Fig. 9. Schematic diagram of microfabrication steps of membrane-supported MEFSS. (a) Sacrificial layer spin. (b) Parylene deposition. (c) Seed layer evaporation. (d) Photoresist spin. (e) Lithography. (f) Gold electroplating. (g) Photoresist removal. (h) Seed layer etch. (i) Coating with Parylene. (j) Removing sacrificial layer. (k) Released FSS.

wafer is coated with a thin photoresist layer and a 10 μm thick layer of Parylene-C is deposited over carrier. Photoresist is used as a sacrificial layer which will be dissolved on the last step to release the Parylene membrane. The structure consists of 7 μm thick elements with feature dimensions as small as 5 μm . Gold electroplating technique is used to achieve thick elements with highly accurate dimensions. First, a thin layer of chrome and gold (500 $^\circ\text{A}$ /500 $^\circ\text{A}$) is evaporated on the Parylene membrane as a seed layer. Next, the seed layer is patterned with the 2D array of FSS elements shown in Fig. 1. A 10 μm thick layer

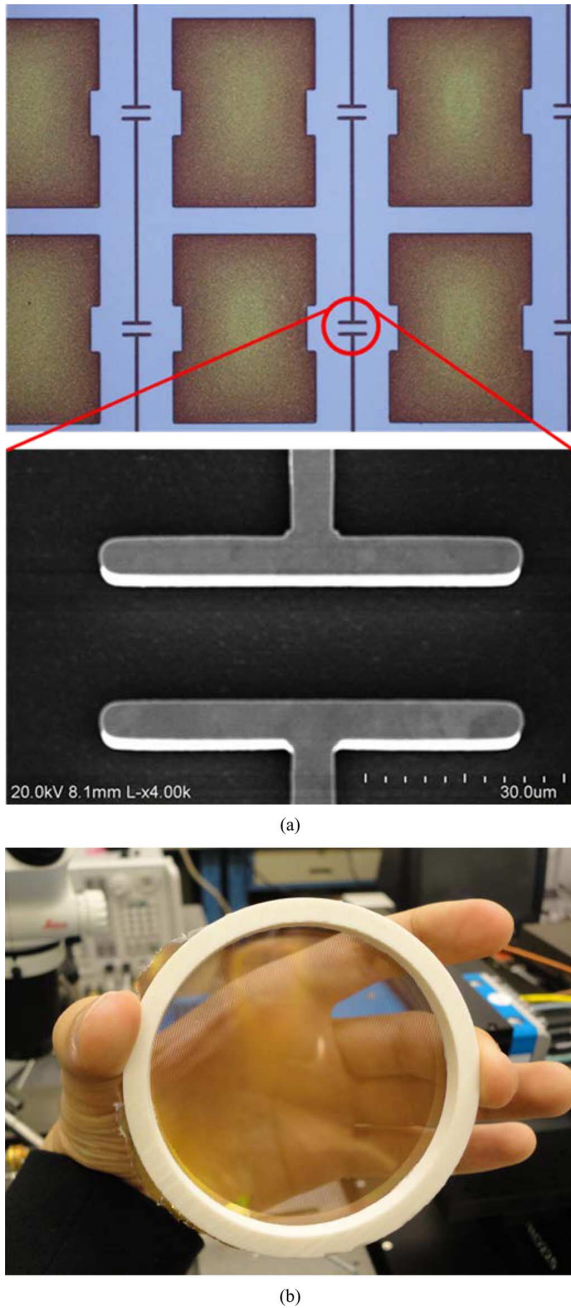


Fig. 10. Photos of fabricated a single-face miniaturized-element FSS. (a) scanning electron microscope image of electroplated gold elements. (b) membrane-supported miniaturized-element FSS after release.

of photoresist AZ 9260 is patterned with the features to allow electroplating up to $7 \mu\text{m}$. Then, the features are electroplated to the desired thickness. After electroplating, the photoresist is dissolved and the seed layer on the previously covered areas is removed by wet etching gold and chrome. Although chrome/gold elements have good adhesion to Parylene, the elements will fall off the membrane when moved and shaken on portable radar systems. To resolve this problem, a thin layer of Parylene ($0.5 \mu\text{m}$) is deposited on the FSS to seal the surface and keep the gold elements in place. This thin Parylene layer increases the capacitance in the circuit model and so the thickness of this layer can be further used as a parameter to



Fig. 11. Free-space measurement setup. FSS screen is placed normal to antennas broadside.

tune the resonant frequencies of the filter. Microscopic images of the fabricated structure are shown in Fig. 10(a).

For the last step, the membrane-supported FSS needs to be detached from the carrier wafer. This is done by dissolving the photoresist underneath the Parylene layer in an acetone solution. Acetone etches the photoresist through cuts made at several locations near the edge of the wafer. After the photoresist is completely etched, the sample is placed in isopropanol to remove any acetone residues on the membrane. A PVC circular support is glued to the FSS and the membrane is cut and released from the carrier as shown in Fig. 10(b).

IV. MEASUREMENT

The transmission response of the fabricated structure is obtained experimentally using the free-space measurement setup shown in Fig. 11. An Agilent N5245 4-port performance network analyzer is used along with OML millimeter-wave frequency extending modules to perform full 2-port S-parameter measurements at Y-band. Two identical pyramidal horn antennas are connected to the frequency extending modules to create a vertically polarized wave front. The beamwidth of the antennas is 13° in the E-plane and 10° in the H-plane and the far-field range is 16 cm. The two antennas are separated by 32 cm and the FSS is placed in between, normal to the broadside of the antennas, equally spaced from each antenna. The antennas foot print at the FSS location is 3.6 cm which is far less than 10 cm diameter of FSS holder. Hence, there is little perturbation due to scattering from the edges of the holder. Transmission (S_{21}) measurements are range gated in the time domain to eliminate multiple reflections from the frequency extending modules. Range gating is achieved by applying the Kaiser-Bessel gating function ($\beta = 15$) centered at 1.07 ns on the time-domain transmission response. The two antennas are aligned for maximum transmission response and system is calibrated using the free-space thru response. Fig. 12 shows the measured transmission response of the membrane-supported MEFSS at normal angle of incidence. The measured response shows a 0.6 dB insertion loss in the 221–223 GHz band and more than 25 dB rejection in the 206–208 GHz band for vertical polarization at a normal angle of incidence.

V. CONCLUSION

A new single face, membrane-supported bandpass MEFSS with an adjacent zero in the transmission response for image re-

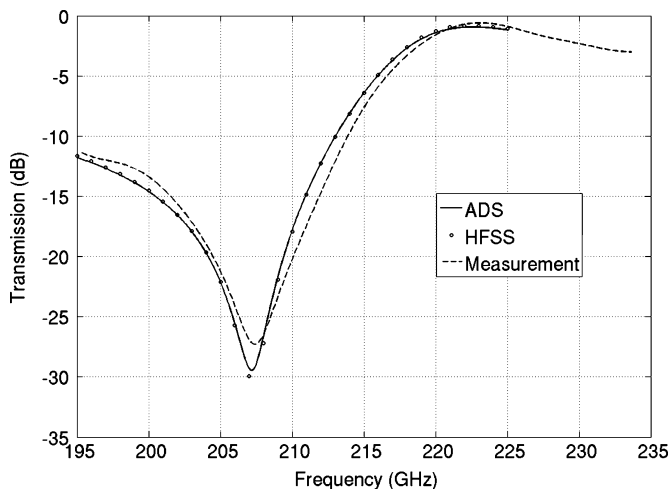


Fig. 12. Measured and simulated transmission response of membrane-supported miniaturized-element FSS.

jection in a 222 GHz radar system is presented. The proposed miniaturized-element patch-wire configuration creates a pole and an adjacent transmission zero filtering response for vertically polarized electromagnetic wave. The location of the pole and the zero can be independently adjusted by varying the geometrical dimensions of the structure. The proposed MEFSS is designed using a simple circuit model and a full-wave analysis which is then realized on a thin Parylene sheet to minimize losses associated with the substrate. The thickness of the metallic traces is optimized to reduce the conductor loss. The membrane-supported MEFSS is fabricated using microfabrication techniques and its transmission response is measured using a free-space measurement setup. Measurement results show that the transmission response has 0.6 dB insertion loss in the pass-band (221–223 GHz) and more than 25 dB rejection around the lower side-band (206–208 GHz) which is in good agreement with numerical simulations of both the structure and its circuit model.

REFERENCES

- [1] M. E. Russell, A. Crain, A. Curran, R. A. Campbell, C. A. Drubin, and W. F. Miccioli, "Millimeter-wave radar sensor for automotive intelligent cruise control (ICC)," *IEEE Tran. Microw. Theory Techn.*, vol. 45, no. 12, pp. 2444–2453, Dec. 1997.
- [2] K. Sarabandi, E. S. Li, and A. Nashashibi, "Modeling and measurements of scattering from road surfaces at millimeter-wave frequencies," *IEEE Trans. Antennas Propag.*, vol. 45, no. 11, pp. 1679–1688, Nov. 1997.
- [3] R. Appleby and R. N. Anderton, "Millimeter-wave and submillimeter-wave imaging for security and surveillance," *Proc. IEEE*, vol. 95, no. 8, pp. 1683–1690, Aug. 2007.
- [4] Y. Li, B. Pan, C. Lugo, M. Tentzeris, and J. Papapolymerou, "A millimeter-wave bandpass waveguide filter using a width-stacked silicon bulk micromachining approach," *IEEE Microw. Wireless Comp. Lett.*, vol. 16, no. 4, pp. 2902–2909, Apr. 2006.
- [5] F. Aryanfar and K. Sarabandi, "Characterization of semilumped CPW elements for millimeter-wave filter design," *IEEE Tran. Microwave Theory Techn.*, vol. 53, no. 4, pp. 1288–1293, Apr. 2005.
- [6] R. Dickie, R. Cahill, H. S. Gamble, and V. F. Fusco, "Spatial demultiplexing in the submillimeter wave band using multilayer free-standing frequency selective surfaces," *IEEE Trans. Antennas Propag.*, vol. 53, no. 6, pp. 1904–1911, June 2005.

- [7] R. Dickie, R. Cahill, H. Gamble, V. Fusco, M. Henry, M. Oldfield, P. Huggard, P. Howard, N. Grant, Y. Munro, and P. Maagt, "Submillimeter wave frequency selective surface with polarization independent spectral responses," *IEEE Trans. Antennas Propag.*, vol. 57, no. 7, pp. 1985–1994, July 2009.
- [8] F. Birbir, J. Shaker, and Y. M. M. Antar, "Chebyshev bandpass spatial filter composed of strip gratings," *IEEE Trans. Antennas Propag.*, vol. 56, no. 12, pp. 3707–3713, Dec. 2008.
- [9] K. Sarabandi and N. Behdad, "A frequency selective surface with miniaturized elements," *IEEE Trans. Antennas Propag.*, vol. 55, no. 5, pp. 1239–1245, May 2007.
- [10] F. Bayatpur and K. Sarabandi, "Multipole spatial filters using metamaterial-based miniaturized-element frequency-selective surfaces," *IEEE Tran. Microw. Theory Techn.*, vol. 56, no. 12, pp. 2742–2747, Dec. 2008.
- [11] M. Moallem and K. Sarabandi, "A single-layer metamaterial-based polarizer and bandpass frequency selective surface with an adjacent transmission zero," in *Int. Symp. Antennas Propag.*, Jul. 2011, pp. 2649–2652.
- [12] M. Moallem and K. Sarabandi, "Y-band phenomenology of indoor environment," in *Int. Symp. Antennas Propag.*, July 2010, pp. 1–4.
- [13] H. Sharifi, R. R. Lahiji, H. Lin, P. D. Ye, L. P. B. Katehi, and S. Mohammadi, "Characterization of parylene-N as flexible substrate and passivation layer for microwave and millimeter-wave integrated circuits," *IEEE Trans. Adv. Packag.*, vol. 32, no. 1, pp. 84–92, Feb. 2009.
- [14] R. E. Collin, *Field Theory of Guided Waves*, 2nd ed. New York: Wiley-IEEE Press, 1990.



Meysam Moallem (S'06) received the B.S. degree in electrical engineering from Sharif University of Technology, Tehran, Iran, in 2008, the M.S. degree in electrical engineering from The University of Michigan at Ann Arbor in 2010, and is currently working toward the Ph.D. degree at The University of Michigan at Ann Arbor.



Kamal Sarabandi (S'87-M'90-SM'92-F'00) received the B.S. degree in electrical engineering from the Sharif University of Technology, Tehran, Iran, in 1980, the M.S. degree in electrical engineering in 1986, and the M.S. degree in mathematics and the Ph.D. degree in electrical engineering from The University of Michigan at Ann Arbor in 1989.

He is currently the Director of the Radiation Laboratory and the Rufus S. Teesdale Professor of Engineering in the Department of Electrical Engineering and Computer Science, The University of Michigan at Ann Arbor. His research areas of interest include microwave and millimeter-wave radar remote sensing, Meta-materials, electromagnetic wave propagation, and antenna miniaturization. He has 25 years of experience with wave propagation in random media, communication channel modeling, microwave sensors, and radar systems and leads a large research group including two research scientists, 12 Ph.D. students. He has graduated 37 Ph.D. and supervised numerous post-doctoral students. He has served as the Principal Investigator on many projects sponsored by the National Aeronautics and Space Administration (NASA), Jet Propulsion Laboratory (JPL), Army Research Office (ARO), Office of Naval Research (ONR), Army Research Laboratory (ARL), National Science Foundation (NSF), Defense Advanced Research Projects Agency (DARPA), and a large number of industries. Currently he is leading the Center for Microelectronics and Sensors funded by the Army Research Laboratory under the Micro-Autonomous Systems and Technology (MAST) Collaborative Technology Alliance (CTA) program. He has published many book chapters and more than 200 papers in refereed journals on miniaturized and on-chip antennas, meta-materials, electromagnetic scattering, wireless channel modeling, random media modeling, microwave measurement techniques, radar calibration, inverse scattering problems, and microwave sensors. He has also had more than 442 papers and invited presentations in many national and international conferences and symposia on similar subjects.

Dr. Sarabandi served as a member of NASA Advisory Council appointed by the NASA Administrator for two consecutive terms from 2006–2010. He is serving as a vice president of the IEEE Geoscience and Remote Sensing Society (GRSS) and is a member of the Editorial Board of the PROCEEDINGS of the IEEE. He was an associate editor of the IEEE TRANSACTIONS ON ANTENNAS AND PROPAGATION and the IEEE SENSORS JOURNAL. He is a member of Commissions F and D of URSI. Dr. Sarabandi was the recipient of the Henry Russel Award from the Regent of The University of Michigan. In 1999 he received a GAAC Distinguished Lecturer Award from the German Federal Ministry for Education, Science, and Technology. He was also a recipient of the 1996 EECS Department Teaching Excellence Award and a 2004 College of Engineering Research Excellence Award. In 2005 he received the IEEE GRSS Distinguished Achievement Award and the University of Michigan Faculty Recog-

niton Award. He also received the best paper Award at the 2006 Army Science Conference. In 2008 he was awarded a Humboldt Research Award from The Alexander von Humboldt Foundation of Germany and received the best paper award at the IEEE Geoscience and Remote Sensing Symposium. He was also awarded the 2010 Distinguished Faculty Achievement Award from the University of Michigan. The IEEE Board of Directors announced him as the recipient of the 2011 IEEE Judith A. Resnik medal. In the past several years, joint papers presented by his students at a number of international symposia (IEEE APS'95,'97,'00,'01,'03,'05,'06,'07; IEEE IGARSS'99,'02,'07,'11 IEEE IMS'01, USNC URSI'04,'05,'06,'10,'11 AMTA '06, URSI GA 2008) have received best paper awards.